Journal of Neuroinflammation

RESEARCH

Open Access

# Extracellular mitochondria contribute to acute lung injury via disrupting macrophages after traumatic brain injury

Yafan Liu[1†], Fanjian Li[1,2†], Lujia Tang[1†], Kaifeng Pang[1†], Yichi Zhang[1†], Chaonan Zhang[1,3], Hui Guo[1,4], Tianrui Ma[1], Xiaoyang Zhang[1], Guili Yang[1], Ying Li[1], Zijian Zhou[1], Hejun Zhang[1,5], Yang Li[6], Ying Fu[7], Jianning Zhang[1*], Jingfei Dong[8,9*] and Zilong Zhao[1,8,10*]

## Abstract

Acute lung injury (ALI) is the most frequently developed complication in patients with severe traumatic brain injury (TBI), but its underlying mechanism remains poorly understood. Here, we report results from a study designed to investigate the mechanistic link between TBI and ALI in mouse models, in vitro experiments, and a patient study, specifically focusing on the role of extracellular mitochondria (exMt). We detected high levels of exMt in the alveolar lavage fluid of patients with TBI. The bronchoalveolar lavage fluid (BALF) of mice subjected to controlled cerebral cortical impact contained $4.2 \pm 1.4 \times 10^4$/μl of exMt. We further showed that non-injured mice infused with exMt intravenously developed pulmonary edema, perivascular accumulation of macrophages, inflammation, and dysfunction. Results from complementary in vitro experiments showed that exMt bound to and were phagocytosed by interstitial macrophages, resulting in autophagic flux reduction and activation of macrophages. The phagocytosis of exMt depended on the CD36 and dynamin mediated pathway, and activation of macrophages depended on exMt-derived reactive oxygen species. This study discovered a novel mechanism by which exMt contribute to the pathogenesis of TBI-induced ALI through macrophages, which are activated, develop dysfunctional autophagy, and become inflammatory after phagocytosis of exMt.

## Introduction

Traumatic brain injury (TBI) is a leading cause of death and disability among young adults, affecting approximately 69 million people per year worldwide [1]. More than 50% of patients with isolated severe TBI develop acute lung injury (TBI-ALI) [2, 3], which can progress to more severe conditions, such as acute respiratory distress syndrome (ARDS) with a mortality rate of 30–40% [4, 5]. TBI-ALI not only exacerbates systemic hypoxia and metabolic dysfunction of the body but also affects cerebral tissue oxygenation and hemodynamics, creating a vicious cycle that promotes secondary cerebral injuries [6, 7]. The question is how a localized brain trauma injures

†Yafan Liu, Fanjian Li, Lujia Tang, Kaifeng Pang and Yichi Zhang contributed equally to this work.

*Correspondence:
Jianning Zhang
jianningzhang@hotmail.com
Jingfei Dong
jfdong@BloodWorksNW.org
Zilong Zhao
zilongzhaotianjin@hotmail.com

Full list of author information is available at the end of the article

**Graphical abstract**

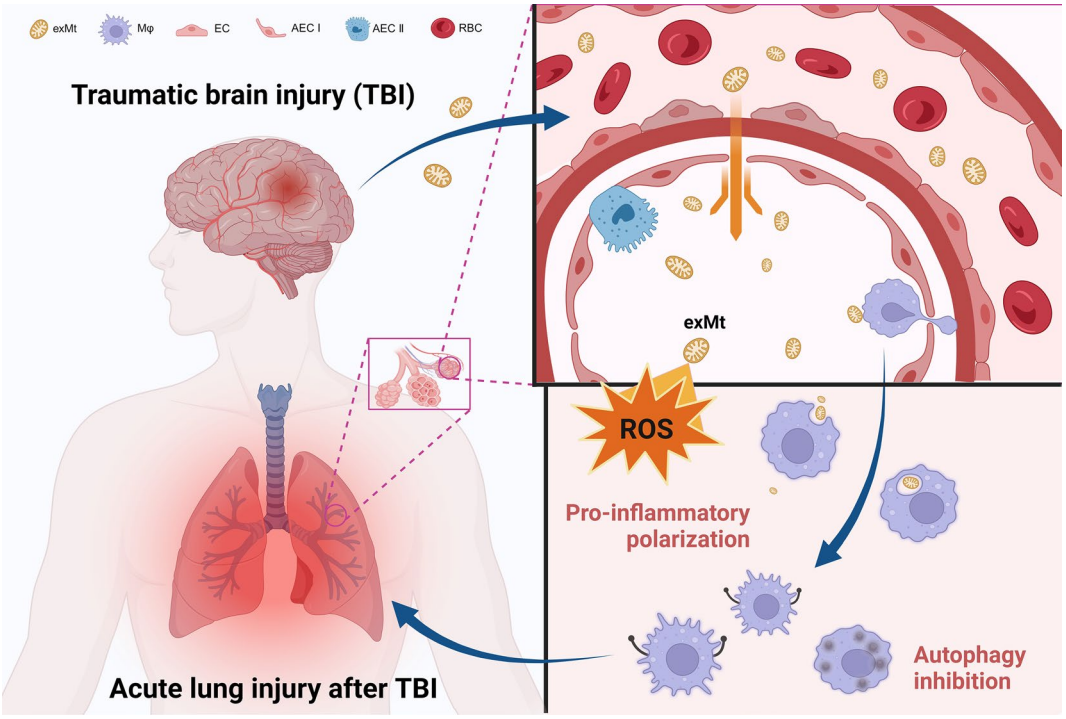


**Keywords** Extracellular mitochondria, Traumatic brain injury, Acute lung injury, Macrophage

remote organs, such as the lungs, and what mediators are involved in the process.

We have previously reported significant presence of anti-brain antibodies, primarily in IgM class in TBI mice [8]. The antibody with the highest titer in these TBI mice is anti-cardiolipin, which is almost exclusively expressed in the inner membrane of intracellular mitochondria, suggesting that mitochondria are released from cells and the anionic phospholipid cardiolipin is transmigrated to the surface of extracellular mitochondria (exMt). These exMt account for more than 50% of anionic phospholipid-expressing extracellular vesicles (EVs) found in these mice. More importantly, exMt promote systemic intravascular coagulation through the surface exposed anionic cardiolipin [8] and activate platelets by reactive oxygen species (ROS) released from these metabolically active exMt [9]. ExMt also activate endothelial cells (ECs) to increase endothelial permeability in the brain and lungs [8, 10], but its underlying mechanism remains largely unknown.

ExMt may cause pulmonary inflammation through several closely related pathways. First, cardiolipin exposed on the surface of exMt serve as the substrate of secreted phospholipase A2 group IIA [11] to induce inflammation [12, 13]. Second, exMt produce ROS that cause local oxidative cellular injuries [9, 14]. Third, disintegrated exMt become mitochondrial damage-associated molecular patterns (mtDAMPs), which are known to propagate inflammation and impair monocyte and T cell functions [15, 16]. However, the pathway linking the procoagulant and proinflammatory activities of exMt to TBI-ALI remains largely unknown. Here, we provide evidence that exMt are closely involved in the pathogenesis of TBI-ALI by interacting with pulmonary interstitial macrophages.

## Materials and methods

### Reagents

Critical reagents and commercial assays are listed in Supplemental TableS1.

### TBI patients

Four patients with traumatic brain injury (TBI) were enrolled based on the following inclusion criteria: (1) TBI confirmed by head computed tomography (CT) or magnetic resonance imaging (MRI) scans during the first 6 h of injury, and (2) 18 to 80 years of age. Patients were excluded when they had (1) spinal cord injury or complex trauma with extracranial injuries; (2) recent neurological disorders, such as stroke; (3) ongoing or recent infections (within a month before admission). A total of 5 patients

were excluded based on the exclusion criteria. TBI severity was categorized by the Glasgow Coma Scale (GCS) as mild (13–15), moderate (9–12), and severe (3–8). Demographics and clinical data were gathered from electronic medical records (Supplemental Table S2). Age- and sex-matched healthy subjects ($n = 12$) were recruited as controls. Due to limited sample size, this patient study was not designed to link exMt to clinical outcomes of patients but to validate data generated from mouse models and lay the foundation for a future clinical study with properly powered sample size. This study was approved by the Ethics Committee of the Tianjin Medical University General Hospital (IRB2023-YX-270-01). Patients or their legal representatives were fully informed about the study's protocol and provided consent.

### Animals

All mouse experiments were approved by the Animal Ethics Committee of the Tianjin Medical University. Male and female C57BL/6J mice were purchased from Beijing HFK BIOSCIENCE CO., LTD (Beijing, China) and were 6–8 weeks old, weighing 22–25 g at the time of experiments. Mice at this age range were chosen to be consistent with the age distribution of TBI patients [3]. Before experiments, the mice were housed in 4–6/cage, with autoclaved wood chip bedding. They were fed a standard rodent chow and had free access to water. The animal facility maintained a 12-hour light/dark cycle at a temperature of 20 ± 2 °C and a humidity of 55 ± 5%.

### Experimental design

In all experiments, mice were randomly assigned to receive various treatments. The outcomes were evaluated by independent researchers, who were blinded to the experimental conditions and group assignments. The schematic representation of the experimental design is shown in Scheme 1.

### Controlled cortical impact (CCI) model of TBI

Mice were subjected to isolated TBI using a digital electromagnetically controlled cortical impact (CCI) device (eCCI-6.3 device, Custom Design & Fabrication, Inc., Sandston, VA, USA) [17]. Briefly, a mouse was anesthetized with 4% isoflurane in 70% $N_2O$ and 30% $O_2$ (0.8 L/min) and remained under anesthesia with 2% isoflurane (0.8 L/min) during TBI. The anesthetized mouse was placed on a stereotactic platform (RWD Life Science Co., Ltd., Shenzhen, China) and trepanned with a 3.0 mm diameter hole on the right between bregma and lambda and lateral to the sagittal suture with the dura mater intact after removing fur from the head. A single force calibrated to the depth of 1.8 mm and velocity of 4.5 m/s for 200 ms was applied to the brain. The scalp was closed immediately after TBI with 6 – 0 silk sutures. The mouse was placed on a heating pad to maintain body temperature for 30 min post-injury and then housed individually in a cage. All TBI mice were closely monitored for the duration of apnea and any signs of distress or complications. Sham mice underwent identical surgery without CCI.

### ExMt isolation

The exMt were isolated from mouse brains using the Qproteome mitochondria isolation kit (Qiagen, Hilden, Germany) and bronchoalveolar lavage fluid (BALF) of TBI mice using a mitochondria isolation kit (Miltenyi, Bergisch Gladbach, Germany). The brains were dissected aseptically from non-injured mice with age matching TBI mice, homogenized, and suspended in the lysis buffer. After a 10-minute incubation at 4℃, the brain homogenates were centrifuged at 1,000 g for 10 min at 4℃. The pellets were resuspended in the disruption buffer and centrifuged at 6,000 g for 10 min at 4℃ to collect the supernatant. The supernatant was collected, resuspended in phosphate-buffered saline (PBS), and centrifuged at

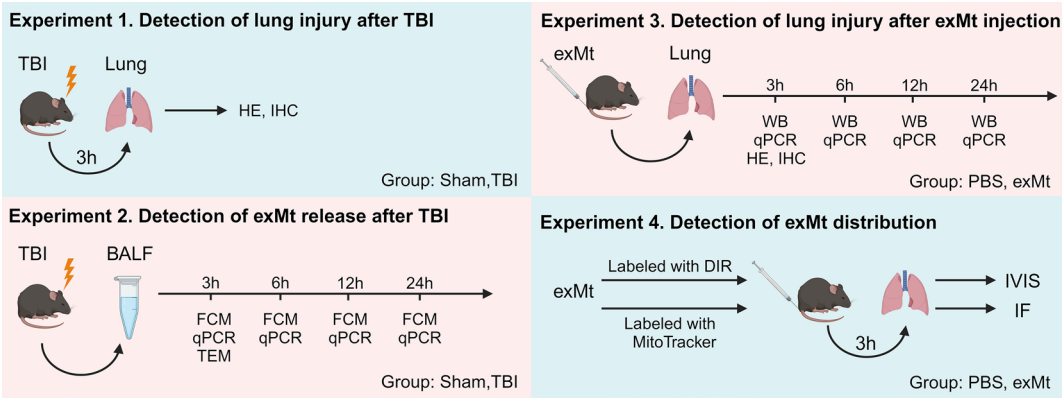


**Scheme 1** Schematic diagram of time points for animal experiments of this study. TBI, traumatic brain injury; HE, hematoxylin and eosin; IHC, immunohistochemistry; FCM, flow cytometry; qPCR, quantitative polymerase chain reaction; TEM, transmission electron microscopy; WB, western blot; IVIS, in vivo imaging system; IF, immunofluorescence

6,000 g for 10 min at 4℃ to collect exMt pellets. On average, approximately $5 \times 10^8$ exMt were obtained from each mouse brain using this method, as quantified using flow cytometry (Supplemental Methods). The exMt isolation from BALF were analyzed for size by nanoparticle tracking analysis (NTA) and ATP (Adenosine Triphosphate) production to compare with exMt isolation from brain (Supplemental methods).

#### ExMt adaptive transfer model

An adaptive transfer model was employed to specifically examine the effects of exMt without the confounding influence of TBI [8]. Briefly, C57BL/6J mice were infused through the tail vein with a single dose of $3 \times 10^7$ exMt (in 150 μL) enriched from the brains of non-injured mice using the Qproteome Mitochondria Isolation Kit (Qiagen, Hilden, Germany) This dose was chosen based on the peak exMt counts detected in plasma samples of TBI mice at 3 h post-injury [8]. Control mice received an equal volume of the vehicle PBS. Blood, BALF, and organ samples were harvested following euthanasia under anesthesia at 3, 6, 12, and 24 h post-infusion for laboratory assays and histopathology.

#### Cell culture

We used cells from three clonal lines (ATCC, Manassas, VA, USA) for in vitro experiments: (1) the mouse macrophage line RAW264.7, derived from BALB/c mice with tumor induced by Abelson murine leukemia virus [18], (2) the endothelial cell line bEnd.3 derived from mouse brain microvessels [19], and (3) the human monocyte line THP-1 derived from an acute monocytic leukemia patient [20]. RAW264.7 cells and bEnd.3 cells were cultured in high-glucose Dulbecco's Modified Eagle's medium (DMEM; Gibco, New York, USA). THP-1 cells were cultured in RPMI 1640 medium (Gibco). Both media were supplemented with 10% fetal bovine serum (FBS). These cells were grown at 37℃ in a 5% $CO^2$ incubator (ThermoFisher, Waltham, Massachusetts, USA).

#### Phagocytosis of ExMt by macrophages

RAW264.7 macrophages were incubated with exMt at a cell-to-exMt ratio of 1:100 for 30 min at 37°C in the presence and absence of either 80 μM dynasore or 10 μM Rapamycin (RAPA) for 30 min before incubation with exMt. For species-crossover experiment, the human THP-1 cells were incubated with mouse exMt for 60 min at 37 °C followed by incubation with 1% trypsin for 10 min to remove surface-bound exMt adherent to the surface of THP-1 macrophages. The cells were then extensively washed with PBS, resuspended in PBS, and subjected to further testing.

Additional details regarding the in vitro experiments, including Endothelial permeability assay, immunoblotting, qPCR, and ELISA are provided in the supplementary methods.

#### Collection of bronchoalveolar lavage fluid (BALF) and lung histopathology

After a mouse was anesthetized using isoflurane, as described earlier, the trachea was surgically exposed, intubated with a 23-gauge lavage tube, and lavaged three times with 1 ml of sterile PBS. After a 30-second dwell time for each lavage, the fluid was gently aspirated using a 1 ml syringe. For patients, BALF collected at the patient's bedside was immediately placed on ice and transported to the laboratory within 3 h. The BALF was passed through a 40-μm nylon filter and centrifuged at 1,000 g for 10 min at 4 °C to obtain the supernatant, which was centrifuged at 6,000 g for 10 min at 4 °C to collect pellets for further analyses.

For histopathology, the mouse was anesthetized by isoflurane overdose and then euthanized by cervical dislocation. Immediately after euthanasia, the chest was opened to allow cardiac puncture to perfuse 20 ml of cold PBS through the right ventricle to remove blood from the vasculature. After perfusion, the lungs were removed and then rinsed with PBS, fixed in 4% paraformaldehyde, paraffin-embedded, and processed into 3 μm sections. These sections were stained with hematoxylin and eosin. The degree of lung injury was determined using a semiquantitative scoring system by an investigator blinded to the treatment group [21].

Additional details regarding the experimental methods, including Pulmonary function test, In vivo imaging system, Evans Blue Dye Extravasation, Immunohistochemistry, Immunofluorescence imaging, and Hematoxylin and Eosin Staining, are provided in the supplementary methods.

#### Flow cytometry

Flow cytometry (FACS Forttesa, Becton Dickinson, New Jersey, USA) was used for detecting: (1) ExMt in plasma samples of TBI patients and mice subjected to CCI [8]. Briefly, samples were incubated with MitoTracker Green (100nM, Invitrogen, Carlsbad, California, United States) and BV421-Annexin V (5 μl in 100 μl cell suspension, Biolegend, San Diego, California, USA) for 30 min at room temperature to specifically detect exMt that also expressed anionic phospholipids. To determine the cellular origin of exMt, they were individually incubated with three distinct antibodies: Alexa Fluor® 488-anti-NSE (neuron-specific enolase, 1:100 dilution, Biolegend, San Diego, California, USA), PE/Cyanine7-anti-CD144 (VE-cadherin, 1:100 dilution, Biolegend, San Diego, California, USA), and PE-anti-CD41 (the integrin α2b, 1:100 dilution, Biolegend, San Diego, California, USA) for 30 min at 37 °C to detect neuronal, endothelial, and

platelet exMt. All samples were incubated with antibodies for 30 min at 37 °C (2) The interaction of exMt with mouse RAW 264.7 macrophages [18]. Briefly, exMt labeled with MitoTracker Green for 30 min at room temperature (100nM, Invitrogen, Carlsbad, California, USA) were incubated with RAW 264.7 cells for 1 h at room temperature. The exMt-RAW264.7 cell mixture were incubated with a brilliant violet 421-conjugated F4/80 antibody (1 µl in 100 µl cell suspension, Biolegend, San Diego, California, USA, 30 min at atmospheric conditions). The F4/80 antibody binds the macrophage marker EMR1 (EGF-like module-containing mucin-like hormone receptor-like 1). The samples were analyzed using the ImageStream® X Mk II system (Amnis, Seattle, WA, USA) at 60 x magnification to visualize and quantify exMt-macrophage complexes. (3) The phagocytic activity of RAW264.7 macrophages after incubation with 0.5 µm fluorescent red carboxylate-modified polystyrene beads (Sigma-Aldrich, Missouri, USA) for 3 h at 37ºC in a cell incubator. (4) The generation of ROS labeled with DCFH-DA from cardiolipin-expressing exMt detected by 10-N-nonyl acridine orange (Supplemental Methods). Isotype-specific Immunoglobulin Gs (IgGs) were used as antibody controls. Flow cytometric data were analyzed with the FlowJo program 7.6.1 (Tree Star, Ashland, Oregon, USA).

#### Transmission electron microscopy (TEM)

Isolated exMt were incubated with macrophages for 30 min at 37ºC. After being extensively washed with PBS for 5 times, they were fixed with 2.5% glutaraldehyde overnight followed by fixation with 1% osmium tetroxide for 2 h at 4 °C. They were then dehydrated with ethanol and cut into ultrathin Sects. (50–70 nm). The sections were viewed under a transmission electron microscope (Hitachi HT7700, Tokyo, Japan) and photographed using Digital Micrograph software (Gatan Inc., CA, USA).

#### Isolation and quantification of mitochondrial DNA

We used the QIAamp DNA Mini Kit (Qiagen) to isolate DNA from BALF of TBI patients (Supplemental Table S2) and mice, as well as from monocytic THP-1 cells (ATCC, Manassas, VA, USA) that had been incubated with exMt at 37 °C for 60 min. Mitochondrial DNA (mtDNA) was then amplified for isolated DNA using quantitative PCR (qPCR) by synthetic primers (Supplemental Table S3) and the SYBR Green PCR Master Mix (Invitrogen, Carlsbad, California, US) through 40 cycles of 95 °C for 15 s and 60 °C for 45 s after initial denaturation at 95 °C for 30 s. The qPCR standard was mtDNA from human umbilical vein endothelial cells (HUVEC, ATCC, Manassas, VA, US) and the mouse brain at known concentrations of 0.008, 0.04, 0.2, 1 and 5 ng/mL.

#### Statistical analysis

Data were analyzed using SPSS 22.0 statistical software (IBM, Armonk, NY, USA). Results were presented as mean ± SEM. For quantitative data, an initial assessment of data normality was performed by the Shapiro-Wilk normality test. Comparative analyses between two groups were performed using the independent samples t-test and comparisons among results from more than two groups were performed using one-way analysis of variance (ANOVA) followed by post hoc Bonferroni's multiple comparison test. A P value of $< 0.05$ was considered statistically significant.

## Results

#### TBI induced the accumulation of ExMt in BALF and acute lung injury

CCI on a small region of the brain (3 mm in diameter) at the given intensity calibrated to a depth of 1.8 mm and a velocity of 4.5 m/s for a duration of 200 ms caused substantial and localized cortical lesions and bleeding (Fig. 1A, left column). These TBI mice developed ALI, defined by enlarged lungs (Fig. 1A, right column) with extensive pulmonary edema and thickened septa in the alveolar cavity (Fig. 1B) and interstitial neutrophil infiltration, detected by the antibody against myeloperoxidase (MPO, Supplemental Figure S1), and worse lung injury score (Fig. 1B). Immunohistochemistry further showed a significant increase in the numbers of macrophages in the interstitial tissues of the lungs from mice at 3 h post-TBI (Fig. 1C).

We also detected exMt in BALF of TBI mice using complementary techniques. First, transmission electron microscopy (TEM) identified exMt in BALFs of patients with TBI (Fig. 1D, left panel) and mice subjected to CCI (Fig. 1D, right panel). These exMt exhibited a typical double membrane and were measured 100–500 nm in diameter. Nanoparticle tracking analysis (NTA) revealed that the peak diameter of exMt was between 100 and 200 nm (Supplemental Figure S2D). Second, flow cytometry detected MitoTracker Green-labeled exMt in BALFs of TBI patients (Fig. 1E) and mice subjected to CCI (Fig. 1F). In TBI patients, the mean concentration of exMt was $19.6 \pm 10.5 \times 10^4$ exMt/µl, and the longitudinal sampling from mouse BALF showed that exMt reached the highest level of $4.2 \pm 1.4 \times 10^4$ exMt/µl at 3 h post-injury (Fig. 1F). A majority of exMt were annexin V-bound, suggesting that they expressed anionic phospholipids on their surface (Supplemental Figure S3B). For the mouse experiments, we were able to collect blood samples at 3, 6, 12, and 24 h post-TBI to allow us to longitudinally follow the dynamic changes in levels of circulating exMt and link these changes to the progressive injury to the lungs. The time points of longitudinal sampling were chosen based on our early observation that (1) plasma exMt reached

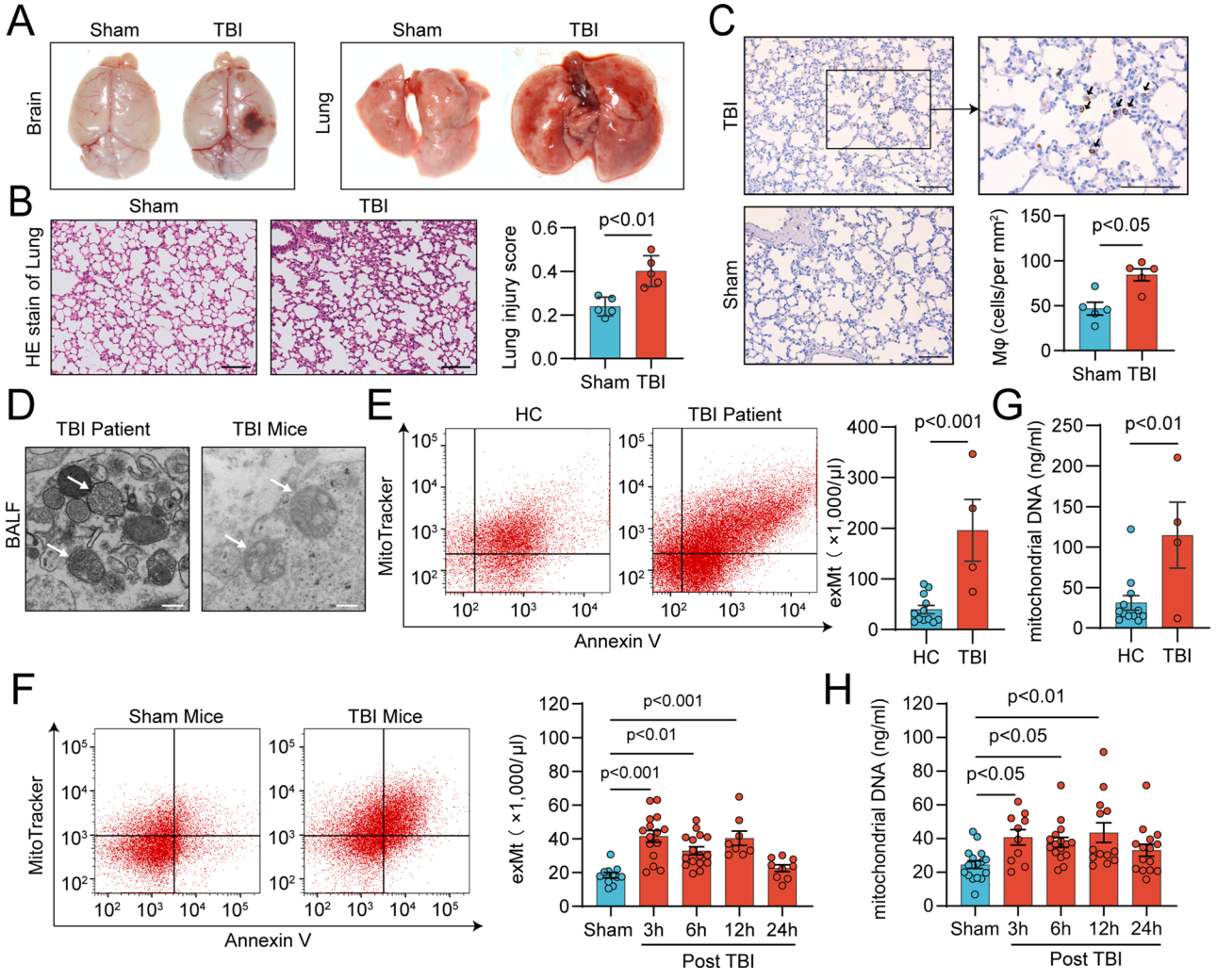


**Fig. 1** TBI induced acute lung injury and exMt accumulation in BALF. (**A**) Visible cerebral damage in the right parietal lobe and hemorrhage in lung tissue. (**B**) Representative H&E images (scale bars: 100 μm) for lung injury at 3 h after CCI compared with Sham surgery and ALI score ($n = 5$/group, paired t test). (**C**) Representative immunohistochemical images of CD68 positive cells (black arrow) in lung tissues (scale bars: 100 μm) and related statistical analysis ($n = 5$/group, paired t test). (**D**) Representative TEM images of exMt in BALF of TBI mice and TBI patients. exMt (left panel, white arrow) in the BALF of clinical TBI patients (scale bars: 0.2 μm); exMt (right panel, white arrow) in normal form in the BALF of TBI mice model (scale bars: 0.2 μm). (**E**) Changes of exMt in BALF samples from healthy humans and TBI patients ($n = 4$ and 12/group, paired t test). (**F**) Changes of exMt in BALF samples from TBI and Sham mice over time ($n = 8$–16/group, one-way ANOVA). (**G**) mtDNA detected in BALF samples from healthy humans and TBI patients ($n = 4$–12/group, paired t test). (**H**) mtDNA detected in BALF samples from TBI and Sham mice over time ($n = 10$–17/group, one-way ANOVA)

the peak levels at 3–6 h followed by a gradual decline [8, 22] and (2) significant lung injury reaches its peak severity at 4 hours post-injury but persists up to 24 h after TBI [23]. For data validation, we also detected elevated levels of mitochondria-specific DNA in BALF samples from TBI patients (Fig. 1G) and mice subjected to CCI (Fig. 1H). Some of the exMt found in the BALF of TBI mice were also labeled with markers for neurons (NSE), endothelial cells (CD144), and platelets (CD41) (Supplemental Figure S4). Third, these exMt were metabolically active in producing ATP (Supplemental Figure S5A) and ROS (Supplemental Figure S5B). Fourth, both female and male mice subjected to TBI had comparable BALF levels of exMt (Supplemental Figure S6A). Together, these results demonstrate that (1) isolated TBI caused ALI that was characterized by pulmonary edema and macrophage/neutrophil infiltration to the interstitial space of the lungs, (2) exMt were detected in BALF samples from TBI patients and C57BL/6J mice exposed to TBI, (3) exMt found in BALF derived from the brain, endothelial cells, and platelets, and (4) Sex did not appear to significantly influence the release of exMt following TBI.

### ExMt caused lung injury in mice independent of traumatic insults

The detection of macrophages and exMt in BALF samples from TBI mice raised the question of whether ROS-generating exMt and mitochondrial DNA, both are

highly pro-inflammatory [24], contribute to the development of ALI during acute TBI. We used an adaptive transfer model [8, 22] to investigate this possibility because this model can exclude the confounding influence of trauma to the brain (e.g., TBI-induced sympathoadrenal activation [25]). Specifically, non-injured mice were infused intravenously with $3 \times 10^7$ exMt/mouse of isolated exMt (to be consistent with the number of exMt found in the peripheral blood of TBI mice) and were examined 3 h post-infusion. The exMt extracted from mouse brains using the commercial kit retained their structural integrity and metabolic activity as those found in BALF samples of TBI mice (Supplemental Figure S2). Several lines of evidence from this study support a causal role of exMt in TBI-ALI. First, the lung tissue from exMt-infused mice had thickened alveolar walls, infiltrated with inflammatory cells, and had worse lung injury score as compared to mice receiving an equal volume of PBS (Fig. 2A), without significant differences between female and male mice (Supplemental Figures S6B and D). Second, exMt-infused mice had a greater wet-dry weight ratio of the total lungs (Fig. 2B), indicative of pulmonary edema, and more proteins in BALF (Fig. 2C), indicative of vascular leakage, as compared to mice receiving PBS. Third, the pulmonary function test found mice receiving exMt had markedly increased inspiratory resistance (RL)

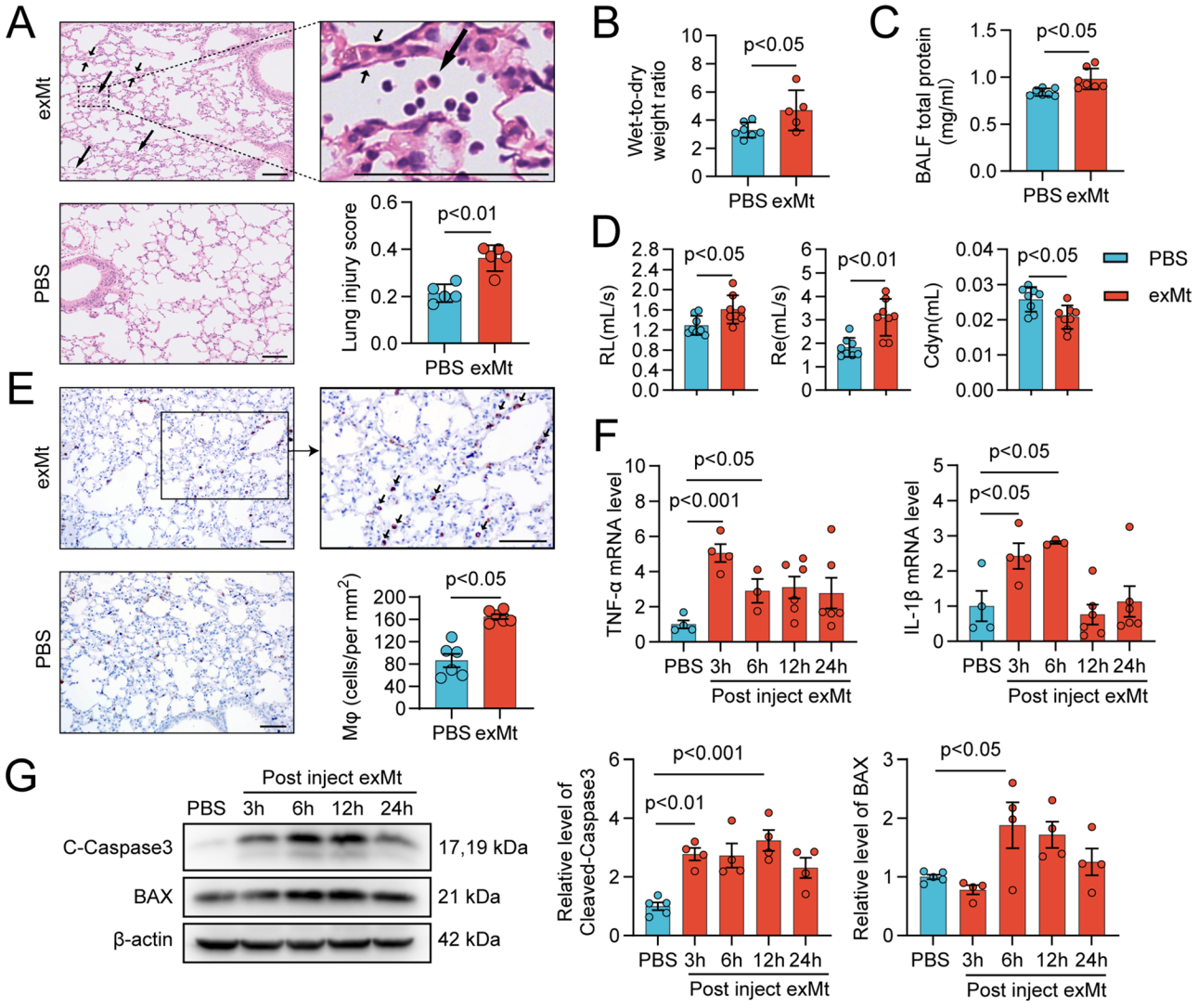


**Fig. 2** ExMt caused lung injury in mice independent of traumatic insults. (**A**) Representative images of H&E staining for lung tissues (scale bars:100 μm) with thickened alveolar wall (short arrow), the infiltration of inflammatory cells (long arrow) and ALI score ($n = 5$/group, paired t test). (**B**) Lung wet/dry tissue weight ratios ($n = 5$–7/group, paired t test). (**C**) BALF total protein concentration ($n = 7$/group, paired t test). (**D**) The lung function of mice was measured via the AniRes 2005 system ($n = 8$, paired t test). (**E**) Representative immunohistochemical images of CD68 positive cells in lung tissues (scale bars: 100 μm) and related statistical analysis ($n = 6$/group, paired t test). (**F**) The expression levels of inflammatory markers of lung tissue were measured by RT-qPCR ($n = 3$–6/group, one-way ANOVA). (**G**) Protein levels of Cleaved caspase3, BAX and β-actin were expressed in lung and related statistical analysis ($n = 4$–5/group, one-way ANOVA)

and expiratory resistance (Re) but reduced dynamic lung compliance (Cdyn, Fig. 2D). Fourth, macrophage infiltration was increased in the interstitial tissue of the lungs from exMt-infused mice (Fig. 2E), with comparable levels between female and male mice (Supplemental Figures S6C and E). Fifth, the quantitative PCR detected higher expressions of the pro-inflammatory factors TNF-α and IL-1β in the lung tissue of TBI mice than control mice (Fig. 2F). Finally, immunoblots detected increased levels of cleaved-caspase-3 and pro-apoptotic protein BAX in the lung tissue of exMt-infused mice (Fig. 2G). We specifically selected caspase 3 and BAX as markers for apoptosis because (1) they are the most common apoptosis markers used in animal study, thus allowing us to compare our results to other reported in the literature, (2) caspase-3 is a general apoptosis marker without be limited to specific pathways (e.g., vs. caspase-12), and (3) the two markers define the progression of apoptosis.

#### ExMt disrupted the endothelial barrier

We infused DiR-labeled exMt into TBI and Sham mice and detected, in real time, the greater accumulation of the labeled exMt in the lungs of TBI mice than those of Sham mice using an in vivo imaging system (IVIS, Fig. 3A). The finding was further supported by additional results. First, exMt labeled with the MitoTracker Green accumulated in interstitial tissue of the lungs detected by immunofluorescence (Supplemental Figure S7). Second, cultured endothelial b.End3 cells, which derived from a clonal endothelial cell line [26], increased permeability to 10 kDa FITC dextran after incubation with exMt for 3 h in vitro (Fig. 3B) and enhanced Evans blue extravasation in the lungs of exMt-infused mice (Fig. 3C) as compared to mice infused with PBS. Third, immunoblots (Fig. 3D) and immunofluorescent staining (Fig. 3E) detected the reduced expression of the tight junction protein Occludin in endothelial cells of the lungs from mice infused with exMt. Additionally, both female and male mice injected with exMt exhibited comparable severity of pulmonary vascular permeability (Supplemental Figure S6F). These results demonstrate that exMt disrupted the endothelial integrity without sex-dependent variation, transmigrated through the endothelium, and caused inflammation in the perivascular tissue of the lungs.

#### Pulmonary macrophages phagocytosed ExMt

When infused into non-injured mice through the tail vein, the MitoTracker Deep Red-labeled exMt transmigrated to and colocalized with macrophages in the interstitial tissue of the lungs (Fig. 4A). Consistent with the in vivo observation, exMt rapidly bound to RAW264.7 cells in vitro in a concentration-dependent manner (Fig. 4B). When macrophages were incubated with exMt for 1 h at 37℃, followed by extensive washing and processed for TEM, we found that macrophages formed pseudopodia that interact with exMt (Fig. 4C and Supplemental Figure S8). Furthermore, in a species-crossing experiment, where we incubated exMt from mouse brains with human monocytic THP-1 cells for 60 min at 37℃, followed by treatment with 1% of trypsin to remove surface-bound exMt, mouse mtDNA was amplified from THP-1 cells (Fig. 4D). Developmental endothelial locus-1 (Del-1) promoted the binding of exMt to RAW264.7 cells in vitro in a concentration-dependent manner (Supplemental Figure S10A) and reduced levels of mtDNA in plasma samples of mice infused with exMt (Supplemental Figure S10B). Del-1 has been shown to promote the phagocytosis of exMt by serving as a coupling factor to capture anionic phospholipid-expressing exMt to monocytes/macrophages to facilitate phagocytosis [27]. The binding of exMt to macrophages was blocked by CD36 antibody (Supplemental Figure S10C). CD36 is the main scavenging receptor that promotes lipid phagocytosis [28]. Together, these data suggest that macrophages phagocytosed exMt in the interstitial space of the lungs.

#### Phagocytosed ExMt activated macrophages

When examined 3 h after infusion, the lungs of mice infused with $3 \times 10^7$ of exMt contained increasing numbers of proinflammatory macrophages defined by CD86 expression and decreasing levels of anti-inflammatory macrophages defined by CD206 (Fig. 5A **and B**). These in vivo observations were supported by the in vitro detection of increased pro-inflammatory macrophages defined by CD86 expression through flow cytometry (Fig. 5C). The exMt-treated RAW264.7 macrophages also enhanced the mRNA expression of the proinflammatory cytokine IL-1 and TNF-α (Fig. 5D) and increased the release of these cytokines into the supernatant (Fig. 5E). This proinflammatory response of RAW 264.7 cells to exMt stimulation was not observed in cells treated with exMt in the presence of dynasore, which inhibits the GTPase dynamin-medicated endocytosis of extracellular vesicles (Supplemental Figure S11) [29]. Furthermore, exMt-stimulated RAW 264.7 cells increased their phagocytic activity defined by their increased uptake of fluorescent microspheres (Fig. 5F). These results demonstrate that macrophages transmigrated to the pulmonary interstitial space during acute TBI and phagocytosed exMt through the dynamin-mediated pathway and became activated to release pro-inflammatory cytokines.

#### ExMt-derived ROS inhibits autophagy and promotes mTOR-dependent macrophage activation in RAW264.7 cells

Autophagy is an intracellular process to remove damaged organelles and can therefore downregulate excessive inflammatory activation of macrophages [30–32].

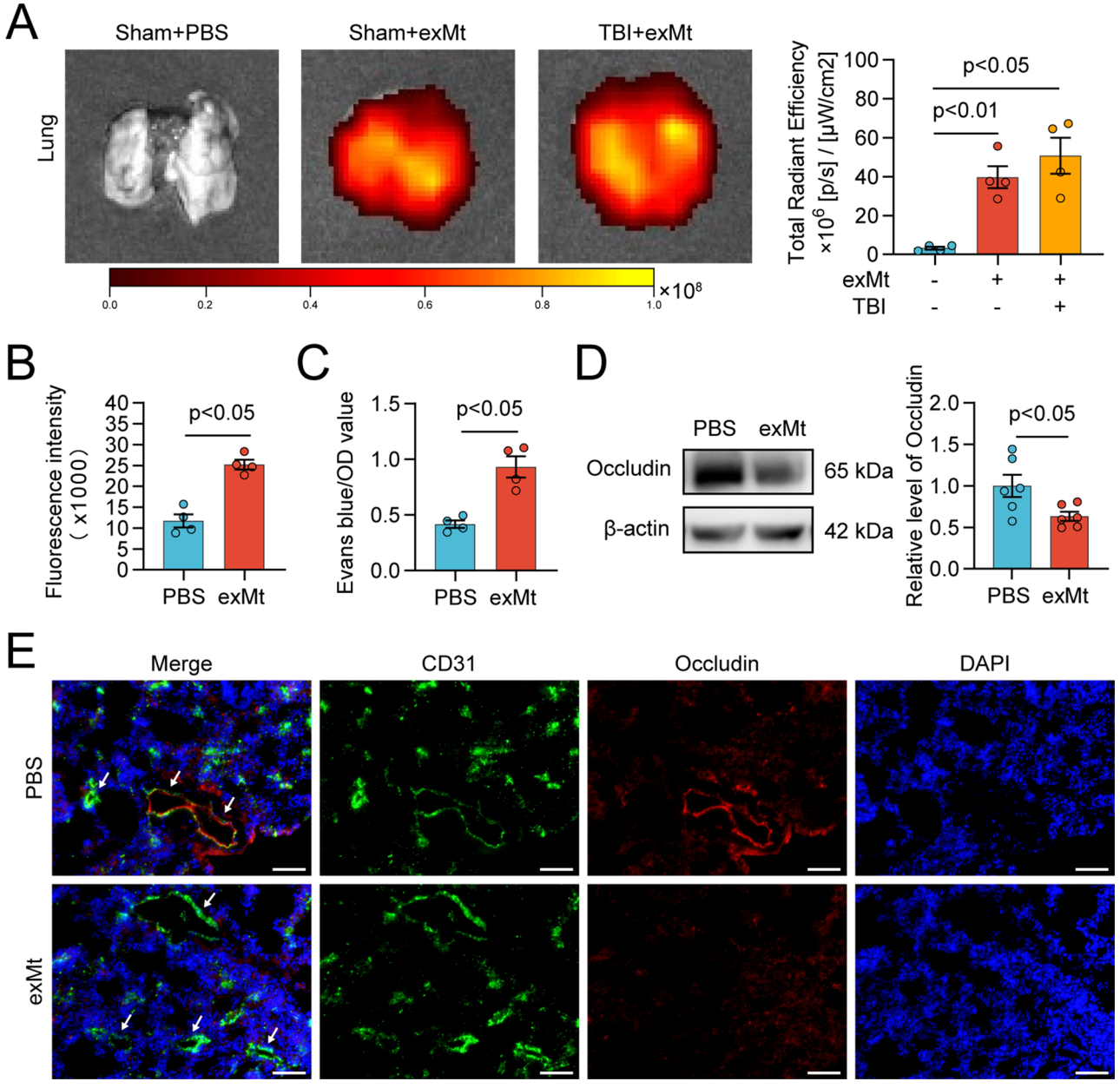


**Fig. 3** ExMt disrupted endothelial barrier. (**A**) Representative images of lung were captured after DiR-labeled exMt (red) injection via in vivo imaging system (IVIS) ($n=4$/group, one-way ANOVA). (**B**) The endothelial permeability was assessed by measuring trans-endothelial leakage of FITC-dextran (10 kDa, $n=4$/group, paired t test). (**C**) Statistical analysis of Evans blue extravasation test in mice lung ($n=4$/group, paired t test). (**D**) Representative western blotting bands and densitometric quantifications of Occludin ($n=6$/group, paired t test). (**E**) Representative immunofluorescence images of Occludin staining in lung tissue (scale bars:100 μm)

Phagocytosed exMt may therefore trigger the process of autophagy to remove exMt to restore cellular homeostasis. Because exMt expressed surface exposed cardiolipin, which activates a specific type of autophagy called mitophagy [33], We found that RAW264.7 cells incubated with exMt for 3 h had the elevated expression of p62 and a reduced LC3II/I ratio, indicating that autophagy was inhibited. This autophagy inhibition was not detected in cells treated with exMt together with dynasore (Fig. 6A), which prevents exMt phagocytosis. Since these exMt were metabolically active to generate ROS (Supplemental Figure S12A), which is known to regulate autophagy [34, 35], we also investigated whether ROS was responsible for inhibiting the autophagic activity of the macrophages. We found that exMt fixed with 4% of polyformaldehyde, which maintained the structural integrity of exMt but made them metabolically inert, did not inhibit the autophagic activity of the host macrophages (Fig. 6B).

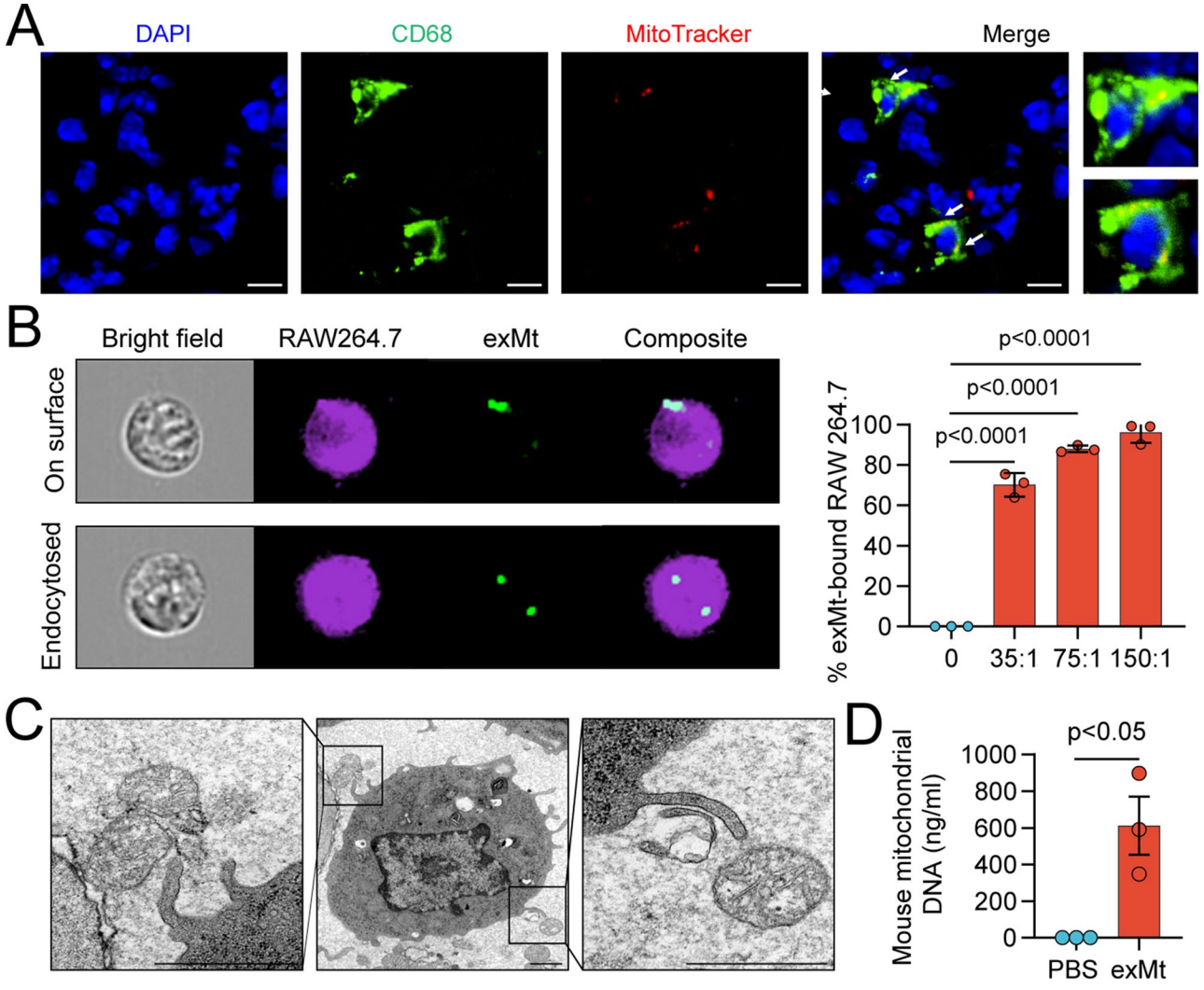


**Fig. 4** Pulmonary macrophages phagocytosed exMt. (**A**) The confocal laser scanning microscope micrographs show that the exMt labeled with MitoTracker are internalized by macrophages (white arrow, scale bars:100 μm, MitoTracker Deep Red: red, CD68: green, DAPI: blue). (**B**) Amnis® flow cytometric images show exMt binding a macrophage (top panel), endocytosed by a macrophage (bottom panel), after 30 min co-incubation at 37 °C (representative images from 20,000 images randomly selected), as shown by a representative histogram in a concentration-dependent manner ($n = 3$/group, one-way analysis of variance). (**C**) exMt bonded to RAW264.7 cells under transmission electron microscopy (scale bars: 2 μm). (**D**) Macrophages internalized exMt ($n = 3$/group, paired t test), as determined by the presence of mouse mitochondrial DNA in mouse exMt-treated human macrophage that were trypsinized to remove surface-bound exMt

Similarly, macrophages treated with exMt together with 50 μM of the cell permeable N-acetyl cysteine (NAC), which quenched ROS (Supplemental Figure S12B), also had a less degree of autophagy inhibition (Fig. 6C). NAC also downregulated the release of proinflammatory cytokines (Fig. 6D) and CD86 expression (Fig. 6E) on exMt-treated macrophages. These results indicate that ROS generated by exMt was responsible for the proinflammatory transformation and autophagy inhibition of exMt-phagocytosed macrophages. Consistent with this possibility, the inhibition of the basal levels autophagy activity of RAW264.7 cells by metabolically active exMt was reversed by the autophagy activator rapamycin (Fig. 6F), which inhibits mTORC1 (Mechanistic Target of Rapamycin Complex 1) to activate autophagy [36]. As results, rapamycin reduced the CD86 expression (Fig. 6G) and release of pro-inflammatory cytokines into the supernatant (Fig. 6H) from cultured RAW264.7 cells treated with exMt.

## Discussion

We studied on exMt as potential mediators of TBI-induced ALI for several reasons. First, the high incidence of pulmonary pathologies such as ALI in TBI patients suggests a significant yet unexplored link between TBI and acute lung injury. Second, exMt are known to accumulate in organs with relatively slow blood flow, such as the lungs, making them a plausible candidate for

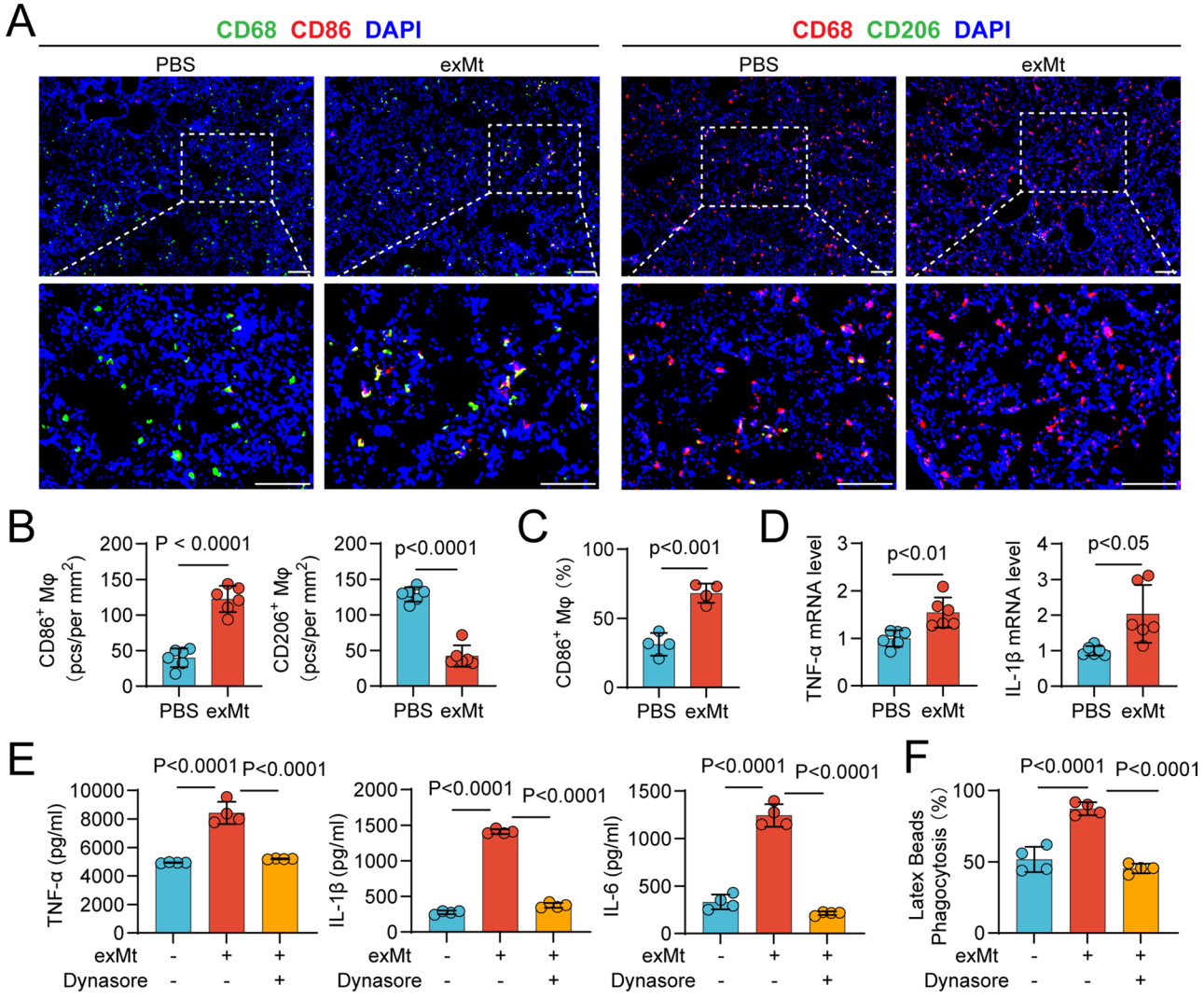


**Fig. 5** Internalized exMt activated macrophages. (**A**) Immunofluorescence images showing an increase in pro-inflammatory macrophages ($CD86^+$) and decrease in anti-inflammatory macrophages ($CD206^+$) within the pulmonary tissue of mice after exMt exposure (scale bars: 100 μm, $n = 6$/group, paired t test). (**B**) The expression levels of inflammatory markers of RAW 264.7 macrophages were measured by qPCR ($n = 5$/group, paired t test). (**C**) Flow cytometry analysis demonstrates an increase in pro-inflammatory macrophages ($CD86^+$) following exMt treatment ($n = 4$/group, paired t test). (**D**) qPCR analysis of pro-inflammatory cytokine mRNA expression in lung tissues exposed to exMt ($n = 6$/group, paired t test). (**E**) ELISA data showing increased levels of IL-1, IL-6, and TNF-α in the supernatants of PBS, exMt and exMt + Dynasore treated RAW264.7 cells ($n = 4$/group, one-way ANOVA). (**F**) Flow cytometry assessment of latex beads phagocytic activity of PBS, exMt and exMt + Dynasore treated RAW264.7 cells ($n = 4$/group, one-way ANOVA)

mediating injury to these organs. Third, exMt possess procoagulant and proinflammatory activities, which are widely considered to be the nature of TBI-induced acute lung injury. Therefore, we designed this study to investigate whether exMt contribute to the development of ALI following TBI.

To elucidate the role of exMt in TBI-induced ALI, we examined acute lung injury in mice subjected to TBI and in those infused with metabolically competent exMt. The findings from mouse models were further validated through in vitro experiments and analysis of samples from a small cohort of TBI patients. These results are consistent with previous clinical observations that patients with severe TBI develop substantial lung injury [37] but also delineate a new pathogenic pathway for TBI-ALI. We made several new observations.

First, morphologically intact exMt were detected in BALF samples from TBI patients and mice subjected to severe TBI (Fig. 1D). These exMt were derived not only from traumatically injured brains but also from endothelial cells and platelets (Supplemental Figure S4). A critical note is that while the primary brain trauma of limited size, the number of neuronal exMt found in peripheral blood samples of TBI mice was comparable to those from endothelial cells and platelets, which are much greater in numbers. This observation is consistent with the fact that

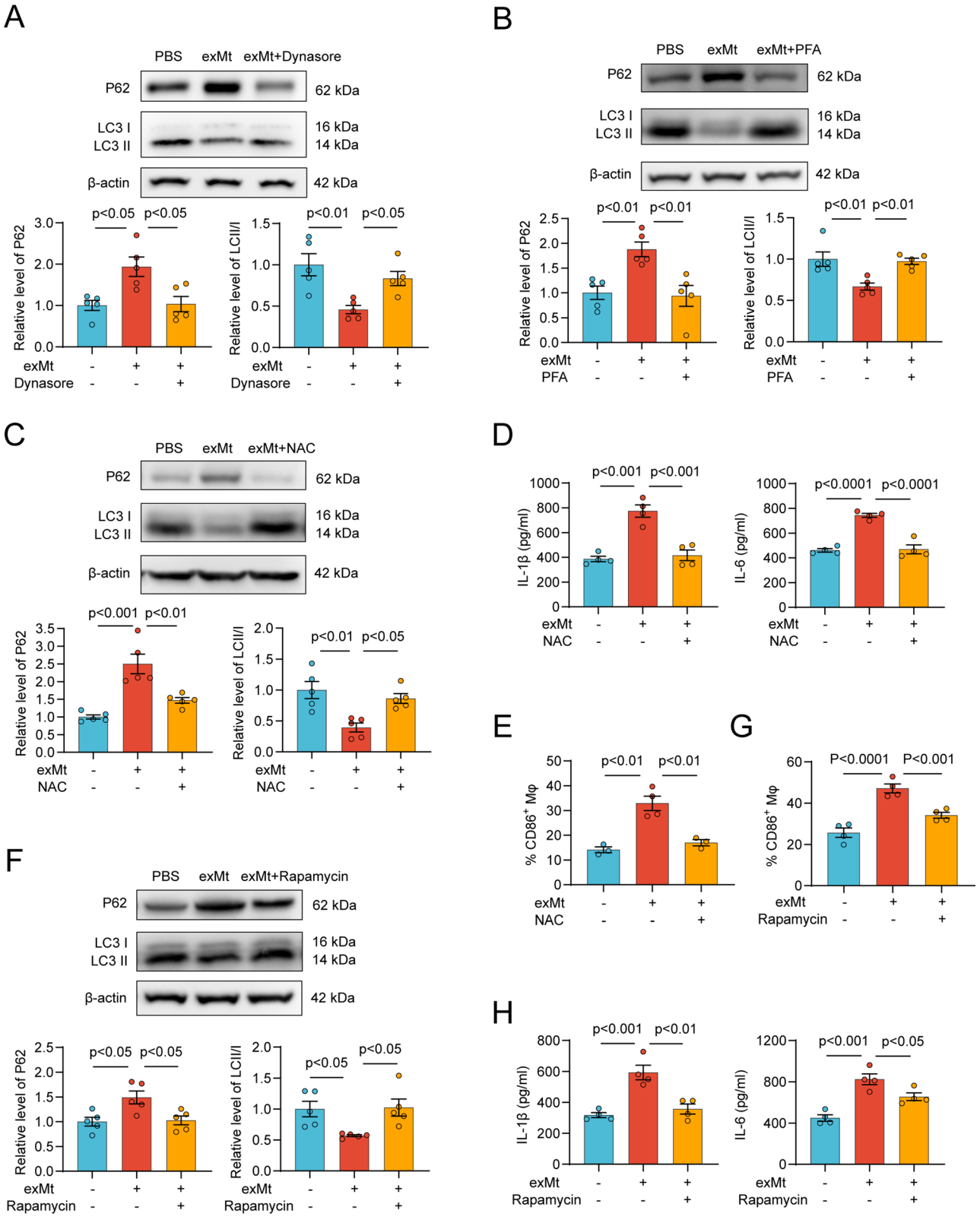


**Fig. 6** (See legend on next page.)

(See figure on previous page.)

**Fig. 6** ExMt-derived ROS inhibits autophagy and promotes mTOR-dependent macrophage activation in RAW264.7 cells. (**A**)Protein levels of P62, LC3B and β-actin were expressed in PBS, exMt and exMt + Dynasore treated RAW264.7 cells and related statistical analysis ($n = 5$/group, one-way ANOVA). (**B**) Protein levels of P62, LC3B and β-actin were expressed in PBS, fresh exMt and fixed exMt-treated RAW264.7 cells and related statistical analysis ($n = 5$/group, one-way ANOVA). (**C**) Protein levels of P62, LC3B and β-actin were expressed in PBS, exMt and exMt + NAC treated RAW264.7 cells and related statistical analysis ($n = 5$/group, one-way ANOVA). (**D**) ELISA measurements of pro-inflammatory cytokines in the culture supernatant of PBS, exMt and exMt + NAC treated RAW264.7 cells treated with exMt and rapamycin ($n = 4$/group, one-way ANOVA). (**E**) Flow cytometry analysis showing a decrease in CD86-positive cells in PBS, exMt and exMt + NAC treated RAW264.7 cells ($n = 3$–4/group, one-way ANOVA). (**F**) Protein levels of P62, LC3B and β-actin were expressed in exMt or exMt + Dynasore treated RAW264.7 and related statistical analysis ($n = 5$/group, one-way ANOVA). Protein levels of P62, LC3B and β-actin were expressed in exMt or exMT + Rapamycin treated RAW264.7 and related statistical analysis ($n = 5$/group, one-way ANOVA). (**G**) Flow cytometry analysis showing a decrease in CD86-positive cells after rapamycin treatment ($n = 4$/group, one-way ANOVA). (**H**) ELISA measurements of pro-inflammatory cytokines in the culture supernatant of RAW264.7 cells treated with exMt and rapamycin ($n = 4$/group, one-way ANOVA)

neuronal cells are highly enriched in mitochondria, containing 2,000–3,000 mitochondria (> 30% of the cell volume) because of their high energy needs [38]. In contrast, endothelial cells and platelets contain less than 5% of those in neurons [11, 39]. We did not test exMt from different cells for contributing to the development of TBI-ALI because there is no evidence that exMt from different cells differ in their structure or express specific makers. However, we speculate that exMt are likely released first from cerebral cells at the site of primary injury in the early time of trauma, followed by exMt from endothelial and blood cells that were subjected to secondary ischemic, hypoxic, and inflammatory injuries. This sequential release of exMt may contribute to the propagation of injury from the brain to remote organs, such as the lungs, which are rich in vasculature with unique blood flow, as we found in this study (Fig. 3A). Unless binding to the endothelium, exMt are rapidly removed from the circulation through the anionic-phospholipid mediated phagocytosis by scavenging factors such as lactadherin. While not investigated, some of the circulating exMt may also be degraded into substructures such as mitochondrial damage-associated molecular patterns (DAMPs). These DAMPs could further propagate inflammation and contribute to the pathogenesis of acute lung injury.

We used an adaptive transfer mouse model to recapitulate the pulmonary injuries in non-injured mice infused with exMt (vascular permeability, pulmonary edema, apoptosis, inflammation and respiratory deficits). Results presented in Fig. 2A-D demonstrate a causal link between exMt and TBI-ALI. This conclusion is supported by previous observations that mitochondrial fragments injected into non-injured mice cause edema, inflammatory responses, and infiltration of alveolar macrophages of the lungs within 3 h post-injection [40, 41]. This time of detecting lung injury is consistent with the time when TBI-ALI developed in mice (Fig. 1B) [23]. Additionally, we did not detect the significant effect of sex on the development and severity of exMt-induced acute lung injury after TBI (Supplemental Figure S6). This observation aligns with the clinical and epidemiological evidence that sex has minimal influence on the rate and severity of TBI-induced pulmonary complications [42, 43]. However, this observation does not exclude the effects of sex hormones on secondary injuries induced by TBI. For example, estrogen has been reported to reduce infection and inflammation associated with TBI [44, 45].

Second, we demonstrated that the phenotypic transformation of macrophages is the key cellular mediator of exMt-induced TBI-ALI. The macrophages accumulated in the perivascular space of the lungs where exMt co-exist, (Figs. 1 and 2) interact with and endocytosed by macrophages through CD36 and dynamin-mediated pathways. This conclusion is supported by: (1) Macrophages captured and engulfed exMt in the perivascular space of the lungs (Fig. 4). (2) ExMt induced a switch in macrophages to a pro-inflammatory type with increasing CD86 and decreasing CD206 expressions in vivo (Fig. 5A-B) and in vitro (Fig. 5C), thus releasing pro-inflammatory cytokines, including IL-1 and TNF-α (Fig. 5D). These inflammatory cytokines mediate macrophage recruitment and adherence [46]. (4) Macrophages simulated with exMt increased their phagocytosis activity (Fig. 5F), suggesting a pro-inflammatory state [47].

Another critical observation is that CD36 on macrophages and cardiolipin on exMt mediated the exMt-macrophage interaction because (1) cardiolipin is the dominant anionic phospholipid expressed on exMt (Supplemental Figure S2B) [8] and (2) the exMt-macrophage interaction was blocked by an antibody against CD36 (Supplemental Figure S10C), which is a scavenger receptor expressed on macrophages and promotes lipid phagocytosis [28]. However, the dynamin-mediated clathrin-endocytosis pathway is also involved in the phagocytosis of exMt and resultant pro-inflammatory response because the dynamin inhibitor dynasore blocked exMt-induced proinflammatory response of macrophages (Fig. 5E-F). These observations suggest that exMt-macrophage interaction depends on both CD36 and dynamin-mediated pathways but how the two systems work jointly remains to be investigated.

Notably, we demonstrated the ability of Del-1 to clear exMt (Supplemental Figure S10A and B), raising an important perspective that anionic phospholipid scavenger molecules, such as Del-1, may reduce TBI-associated lung injury by removing exMt from the circulation. Del-1

has been reported to promote the remission of inflammation in macrophage, and Del-1 deficiency mice had enhanced macrophage polarization [48, 49].

Finally, the metabolic activity of exMt suggests a potential role of ROS in causing autophagy impairment and contributing to the phenotypic transformation of macrophages to proinflammation. This conclusion is supported by: (1) Impaired autophagic flux in macrophages incubated with exMt (Fig. 6A) and its prevention by blocking ROS (Fig. 6B and C). (2) Impaired autophagic flux contributes to a proinflammatory response from exMt-phagocytosed macrophages [47, 50]. (3) The activation of macrophages by exMt was blocked by the autophagy inducer rapamycin or inhibiting mTORC1 (Fig. 6G and H). Given that ROS are known to impair autophagy by activating mTORC1 [51–55], ROS carried by exMt may promote the classical activation of macrophages by impairing mTORC1-regulated autophagic flux.

Our study offers novel insights into exMt's role in TBI-ALI. The study limitations include: (1) this study focused mainly on the acute phase of TBI whereas the long-term effects of exMt were unexplored. For example, the effects of exMt on the cerebral endothelium may enhance TBI-induced brain injury, leading to cognitive decline and behavioral abnormalities. Second, the study was conducted in a controlled experimental setting with limited validation by a small cohort of TBI patients. Further clinical studies are needed to validate the role of exMt through fully powered clinical studies.

In summary, we have shown that exMt were released into BALF and contribute to the pathogenesis of TBI-induced ALI by promoting perivascular accumulation and activation of proinflammatory macrophages that phagocytose exMt. These findings will provide new biomarkers and therapeutic targets for the prevention of TBI-induced secondary lung injury.

## Supplementary Information

The online version contains supplementary material available at https://doi.org/10.1186/s12974-025-03390-x .

Supplementary Material 1

### Author contributions

YFL: conducted experiments, analyzed data, and wrote the manuscript; FJL: performed histopathology and wrote the manuscript; LJT, KFP and YCZ: performed in vitro experiment and analyzed data; CNZ, HG and TRM: performed experiments and analyzed data; XYZ: provided Del-1 and technical support; GLY: designed flow cytometry experiments and analyzed data; YL: provided technical support; ZJZ and HJZ: performed mouse tissue pathology; YL and YF: assisted in data analysis; JZ, JFD, and ZZ: formulated hypothesis, designed the study, and wrote manuscript.

### Funding

This study is supported by the National Natural Science Foundation of China 82022020, 82371376, 81971176 (ZLZ) and 81930031, 81720108015 (JNZ); Natural Science Foundation of Tianjin Municipality 23JCZXJC00330, 21JCYBJC00980 (ZLZ).

### Data availability

No datasets were generated or analysed during the current study.

## Declarations

### Competing interests

The authors declare no competing interests.

### Author details

[1]Department of Neurosurgery and Tianjin Institute of Neurology, Tianjin Medical University General Hospital, Tianjin, China
[2]Department of Neurosurgery, The First Affiliated Hospital of Nanchang Medical College, Nanchang, China
[3]Beijing Neurosurgical Institute, Capital Medical University, Beijing, China
[4]Respiratory and Critical Care Medicine Department, Chest Hospital, Tianjin University, Tianjin, China
[5]Department of Neurosurgery, First Hospital of Qinhuangdao, Qinhuangdao, China
[6]Center of Precision Medicine, Tianjin Medical University General Hospital, Tianjin, China
[7]Department of Neurology, Institute of Neurology of First Affiliated Hospital, Institute of Neuroscience, Fujian Key Laboratory of Molecular Neurology, Fujian Medical University, Fuzhou, China
[8]BloodWorks Research Institute, 1551 Eastlake Avenue East, Seattle, WA, USA
[9]Division of Hematology and Oncology, Department of Medicine, School of Medicine, University of Washington, Seattle, WA, USA
[10]National Key Laboratory of Experimental Hematology, Tianjin, China

Received: 20 October 2024 / Accepted: 20 February 2025
Published online: 04 March 2025

### References

1. Dewan MC, Rattani A, Gupta S, Baticulon RE, Hung YC, Punchak M, et al. Estimating the global incidence of traumatic brain injury. J Neurosurg. 2018; 130:1080–97.
2. Summers CR, Ivins B, Schwab KA. Traumatic brain injury in the united States: an epidemiologic overview. Mt Sinai J Med. 2009;76:105–10.
3. Maas AIR, Menon DK, Adelson PD, Andelic N, Bell MJ, Belli A, Bragge P, Brazinova A, Buki A, Chesnut RM, Citerio G, Coburn M, Cooper DJ, Crowder AT, Czeiter E, Czosnyka M, Diaz-Arrastia R, Dreier JP, Duhaime AC, Ercole A, van Essen TA, Feigin VL, Gao G, Giacino J, Gonzalez-Lara LE, Gruen RL, Gupta D, Hartings JA, Hill S, Jiang JY, Ketharanathan N, Kompanje EJO, Lanyon L, Laureys S, Lecky F, Levin H, Lingsma HF, Maegele M, Majdan M, Manley G, Marsteller J, Mascia L, McFadyen C, Mondello S, Newcombe V, Palotie A, Parizel PM, Peul W, Piercy J, Polinder S, Puybasset L, Rasmussen TE, Rossaint R, Smielewski P, Soderberg J, Stanworth SJ, Stein MB, von Steinbuchel N, Stewart W, Steyerberg EW, Stocchetti N, Synnot A, Te Ao B, Tenovuo O, Theadom A, Tibboel D, Wang WH, Williams L, Wilson K, Yaffe TP. W. Videtta, K.K.W. In, Investigators, Traumatic brain injury: integrated approaches to improve prevention, clinical care, and research, Lancet Neurol, 2017;16:987–1048.
4. Aisiku IP, Yamal JM, Doshi P, Rubin ML, Benoit JS, Hannay J, Tilley BC, Gopinath S, Robertson CS. The incidence of ARDS and associated mortality in severe TBI using the Berlin definition. J Trauma Acute Care Surg. 2016;80:308–12.
5. Ziaka M, Exadaktylos A. Brain-lung interactions and mechanical ventilation in patients with isolated brain injury. Crit Care. 2021;25:358.
6. Robba C, Asgari S, Gupta A, Badenes R, Sekhon M, Bequiri E, Hutchinson PJ, Pelosi P, Gupta A. Lung injury is a predictor of cerebral hypoxia and mortality in traumatic brain injury. Front Neurol. 2020;11:771.
7. Ziaka M, Exadaktylos A. Pathophysiology of acute lung injury in patients with acute brain injury: the triple-hit hypothesis. Crit Care. 2024;28:71.
8. Zhao Z, Wang M, Tian Y, Hilton T, Salsbery B, Zhou EZ, Wu X, Thiagarajan P, Boilard E, Li M, Zhang J, Dong JF. Cardiolipin-mediated procoagulant activity of mitochondria contributes to traumatic brain injury-associated coagulopathy in mice. Blood. 2016;127:2763–72.
9. Zhao Z, Zhou Y, Hilton T, Li F, Han C, Liu L, Yuan H, Li Y, Xu X, Wu X, Zhang F, Thiagarajan P, Cap A, Shi FD, Zhang J, Dong JF. Extracellular mitochondria released from traumatized brains induced platelet procoagulant activity. Haematologica. 2020;105:209–17.

10. Puhm F, Afonyushkin T, Resch U, Obermayer G, Rohde M, Penz T, Schuster M, Wagner G, Rendeiro AF, Melki I, Kaun C, Wojta J, Bock C, Jilma B, Mackman N, Boilard E, Binder CJ. Mitochondria are a subset of extracellular vesicles released by activated monocytes and induce type I IFN and TNF responses in endothelial cells. Circ Res. 2019;125:43–52.
11. Boudreau LH, Duchez AC, Cloutier N, Soulet D, Martin N, Bollinger J, Pare A, Rousseau M, Naika GS, Levesque T, Laflamme C, Marcoux G, Lambeau G, Farndale RW, Pouliot M, Hamzeh-Cognasse H, Cognasse F, Garraud O, Nigrovic PA, Guderley H, Lacroix S, Thibault L, Semple JW, Gelb MH, Boilard E. Platelets release mitochondria serving as substrate for bactericidal group IIA-secreted phospholipase A2 to promote inflammation. Blood. 2014;124:2173–83.
12. Birts CN, Barton CH, Wilton DC. Catalytic and non-catalytic functions of human IIA phospholipase A2. Trends Biochem Sci. 2010;35:28–35.
13. Letsiou E, Htwe YM, Dudek SM. Secretory phospholipase A(2) enzymes in acute lung injury. Cell Biochem Biophys. 2021;79:609–17.
14. Zhang C, Liu C, Li F, Zheng M, Liu Y, Li L, Yang H, Zhang S, Wang C, Rong H, Guo H, Li Y, Li Y, Fu Y, Zhao Z, Zhang J. Extracellular mitochondria activate microglia and contribute to neuroinflammation in traumatic brain injury. Neurotox Res. 2022;40:2264–77.
15. Huber-Lang M, Lambris JD, Ward PA. Innate immune responses to trauma. Nat Immunol. 2018;19:327–41.
16. Munford RS, Pugin J. Normal responses to injury prevent systemic inflammation and can be immunosuppressive. Am J Respir Crit Care Med. 2001;163:316–21.
17. Xiong Y, Mahmood A, Chopp M. Animal models of traumatic brain injury. Nat Rev Neurosci. 2013;14:128–42.
18. Raschke WC, Baird S, Ralph P, Nakoinz I. Functional macrophage cell lines transformed by Abelson leukemia virus. Cell. 1978;15:261–7.
19. Williams RL, Risau W, Zerwes HG, Drexler H, Aguzzi A, Wagner EF. Endothelioma cells expressing the polyoma middle T oncogene induce hemangiomas by host cell recruitment. Cell. 1989;57:1053–63.
20. Tsuchiya S, Yamabe M, Yamaguchi Y, Kobayashi Y, Konno T, Tada K. Establishment and characterization of a human acute monocytic leukemia cell line (THP-1). Int J Cancer. 1980;26:171–6.
21. Matute-Bello G, Downey G, Moore BB, Groshong SD, Matthay MA, Slutsky AS, Kuebler WM. Acute lung injury in animals study, an official American thoracic society workshop report: features and measurements of experimental acute lung injury in animals. Am J Respir Cell Mol Biol. 2011;44:725–38.
22. Tian Y, Salsbery B, Wang M, Yuan H, Yang J, Zhao Z, Wu X, Zhang Y, Konkle BA, Thiagarajan P, Li M, Zhang J, Dong JF. Brain-derived microparticles induce systemic coagulation in a murine model of traumatic brain injury. Blood. 2015;125:2151–9.
23. Kerr NA, de Rivero Vaccari JP, Abbassi S, Kaur H, Zambrano R, Wu S, Dietrich WD, Keane RW. Traumatic brain Injury-Induced acute lung injury: evidence for activation and Inhibition of a Neural-Respiratory-Inflammasome Axis. J Neurotrauma. 2018;35:2067–76.
24. West AP, Shadel GS. Mitochondrial DNA in innate immune responses and inflammatory pathology. Nat Rev Immunol. 2017;17:363–75.
25. Di Battista AP, Rhind SG, Hutchison MG, Hassan S, Shiu MY, Inaba K, Topolovec-Vranic J, Neto AC, Rizoli SB, Baker AJ. Inflammatory cytokine and chemokine profiles are associated with patient outcome and the hyperadrenergic state following acute brain injury. J Neuroinflamm. 2016;13:40.
26. Williams RL, Courtneidge SA, Wagner EF. Embryonic lethalities and endothelial tumors in chimeric mice expressing polyoma virus middle T oncogene. Cell. 1988;52:121–31.
27. Kourtzelis I, Li X, Mitroulis I, Grosser D, Kajikawa T, Wang B, Grzybek M, von Renesse J, Czogalla A, Troullinaki M, Ferreira A, Doreth C, Ruppova K, Chen LS, Hosur K, Lim JH, Chung KJ, Grossklaus S, Tausche AK, Joosten LAB, Moutsopoulos NM, Wielockx B, Castrillo A, Korostoff JM, Coskun U, Hajishengallis G, Chavakis T. DEL-1 promotes macrophage efferocytosis and clearance of inflammation. Nat Immunol. 2019;20:40–9.
28. Balasubramanian K, Maeda A, Lee JS, Mohammadyani D, Dar HH, Jiang JF, St Croix CM, Watkins S, Tyurin VA, Tyurina YY, Kloditz K, Polimova A, Kapralova VI, Xiong Z, Ray P, Klein-Seetharaman J, Mallampalli RK, Bayir H, Fadeel B, Kagan VE. Dichotomous roles for externalized Cardiolipin in extracellular signaling: promotion of phagocytosis and Attenuation of innate immunity. Sci Signal. 2015;8:ra95.
29. Macia E, Ehrlich M, Massol R, Boucrot E, Brunner C, Kirchhausen T. Dynasore, a cell-permeable inhibitor of dynamin. Dev Cell. 2006;10:839–50.
30. Saitoh T, Fujita N, Jang MH, Uematsu S, Yang BG, Satoh T, Omori H, Noda T, Yamamoto N, Komatsu M, Tanaka K, Kawai T, Tsujimura T, Takeuchi O, Yoshimori T, Akira S. Loss of the autophagy protein Atg16L1 enhances endotoxin-induced IL-1beta production. Nature. 2008;456:264–8.
31. Crisan TO, Plantinga TS, van de Veerdonk FL, Farcas MF, Stoffels M, Kullberg BJ, van der Meer JW, Joosten LA, Netea MG. Inflammasome-independent modulation of cytokine response by autophagy in human cells. PLoS ONE. 2011;6:e18666.
32. Nakahira K, Haspel JA, Rathinam VA, Lee SJ, Dolinay T, Lam HC, Englert JA, Rabinovitch M, Cernadas M, Kim HP, Fitzgerald KA, Ryter SW, Choi AM. Autophagy proteins regulate innate immune responses by inhibiting the release of mitochondrial DNA mediated by the NALP3 inflammasome. Nat Immunol. 2011;12:222–30.
33. Chu CT, Ji J, Dagda RK, Jiang JF, Tyurina YY, Kapralov AA, Tyurin VA, Yanamala N, Shrivastava IH, Mohammadyani D, Wang KZQ, Zhu J, Klein-Seetharaman J, Balasubramanian K, Amoscato AA, Borisenko G, Huang Z, Gusdon AM, Cheikhi A, Steer EK, Wang R, Baty C, Watkins S, Bahar I, Bayir H, Kagan VE. Cardiolipin externalization to the outer mitochondrial membrane acts as an elimination signal for mitophagy in neuronal cells. Nat Cell Biol. 2013;15:1197–205.
34. Lee J, Giordano S, Zhang J. Autophagy, mitochondria and oxidative stress: cross-talk and redox signalling. Biochem J. 2012;441:523–40.
35. Filomeni G, De Zio D, Cecconi F. Oxidative stress and autophagy: the clash between damage and metabolic needs. Cell Death Differ. 2015;22:377–88.
36. Lamming DW. Inhibition of the mechanistic target of Rapamycin (mTOR)-Rapamycin and beyond. Cold Spring Harb Perspect Med. 2016;6:a025924.
37. Hu PJ, Pittet JF, Kerby JD, Bosarge PL, Wagener BM. Acute brain trauma, lung injury, and pneumonia: more than just altered mental status and decreased airway protection. Am J Physiol Lung Cell Mol Physiol. 2017;313:L1–15.
38. Misgeld T, Schwarz TL. Mitostasis in Neurons: Maintaining Mitochondria in an Extended Cellular Architecture, Neuron, 2017;96:651–666.
39. Tang X, Luo YX, Chen HZ, Liu DP. Mitochondria, endothelial cell function, and vascular diseases. Front Physiol. 2014;5:175.
40. Zhang Q, Raoof M, Chen Y, Sumi Y, Sursal T, Junger W, Brohi K, Itagaki K, Hauser CJ. Circulating mitochondrial damps cause inflammatory responses to injury. Nature. 2010;464:104–7.
41. Gu X, Wu G, Yao Y, Zeng J, Shi D, Lv T, Luo L, Song Y. Intratracheal administration of mitochondrial DNA directly provokes lung inflammation through the TLR9-p38 MAPK pathway. Free Radic Biol Med. 2015;83:149–58.
42. Robba C., Rebora P., Banzato E., Wiegers E.J.A., Stocchetti N., Menon D.K., Citerio G., Collaborative European NeuroTrauma Effectiveness Research in Traumatic Brain Injury, Investigators P., Incidence, Risk Factors, and Effects on Outcome of Ventilator-Associated Pneumonia in Patients With Traumatic Brain Injury: Analysis of a Large, Multicenter, Prospective, Observational Longitudinal Study. Chest. 2020;158:2292–303.
43. Coimbra R, Hoyt DB, Potenza BM, Fortlage D, Hollingsworth-Fridlund P. Does sexual dimorphism influence outcome of traumatic brain injury patients? The answer is no! J Trauma. 2003;54:689–700.
44. Pittet JF, Hu PJ, Honavar J, Brandon AP, Evans CA, Muthalaly R, Ding Q, Wagener BM. Estrogen alleviates Sex-Dependent differences in lung bacterial clearance and mortality secondary to bacterial pneumonia after traumatic brain injury. J Neurotrauma. 2021;38:989–99.
45. Gubbels Bupp MR. Sex, the aging immune system, and chronic disease. Cell Immunol. 2015;294:102–10.
46. Ott LW, Resing KA, Sizemore AW, Heyen JW, Cocklin RR, Pedrick NM, Woods HC, Chen JY, Goebl MG, Witzmann FA, Harrington MA. Tumor necrosis Factor-alpha- and interleukin-1-induced cellular responses: coupling proteomic and genomic information. J Proteome Res. 2007;6:2176–85.
47. Patoli D, Mignotte F, Deckert V, Dusuel A, Dumont A, Rieu A, Jalil A, Van Dongen K, Bourgeois T, Gautier T, Magnani C, Le Guern N, Mandard S, Bastin J, Djouadi F, Schaeffer C, Guillaumot N, Narce M, Nguyen M, Guy J, Dargent A, Quenot JP, Rialland M, Masson D, Auwerx J, Lagrost L, Thomas C. Inhibition of mitophagy drives macrophage activation and antibacterial defense during sepsis. J Clin Invest. 2020;130:5858–74.
48. Wei X, Zou S, Xie Z, Wang Z, Huang N, Cen Z, Hao Y, Zhang C, Chen Z, Zhao F, Hu Z, Teng X, Gui Y, Liu X, Zheng H, Zhou H, Chen S, Cheng J, Zeng F, Zhou Y, Wu W, Hu J, Wei Y, Cui K, Li J. EDIL3 deficiency ameliorates adverse cardiac remodelling by neutrophil extracellular traps (NET)-mediated macrophage polarization. Cardiovasc Res. 2022;118:2179–95.
49. Kwak N, Lee KH, Woo J, Kim J, Park J, Lee CH, Yoo CG. Del-1 plays a protective role against COPD development by inhibiting inflammation and apoptosis. Int J Mol Sci, 2024;25.
50. Xu Y, Shen J, Ran Z. Emerging views of mitophagy in immunity and autoimmune diseases. Autophagy. 2020;16:3–17.

51. Dobson B. Child and adolescent psychiatry in the undergraduate medical curriculum. Med Educ. 1988;22:301–7.
52. Yalcin S, Marinkovic D, Mungamuri SK, Zhang X, Tong W, Sellers R, Ghaffari S. ROS-mediated amplification of AKT/mTOR signalling pathway leads to myeloproliferative syndrome in Foxo3(-/-) mice. EMBO J. 2010;29:4118–31.
53. Vigneron F, Dos Santos P, Lemoine S, Bonnet M, Tariosse L, Couffinhal T, Duplaa C, Jaspard-Vinassa B. GSK-3beta at the crossroads in the signalling of heart preconditioning: implication of mTOR and Wnt pathways. Cardiovasc Res. 2011;90:49–56.
54. Calamaras TD, Lee C, Lan F, Ido Y, Siwik DA, Colucci WS. The lipid peroxidation product 4-hydroxy-trans-2-nonenal causes protein synthesis in cardiac myocytes via activated mTORC1-p70S6K-RPS6 signaling. Free Radic Biol Med. 2015;82:137–46.
55. Oeing CU, Nakamura T, Pan S, Mishra S, Dunkerly-Eyring BL, Kokkonen-Simon KM, Lin BL, Chen A, Zhu G, Bedja D, Lee DI, Kass DA. Ranek, PKG1alpha Cysteine-42 redox state controls mTORC1 activation in pathological cardiac hypertrophy. Circ Res. 2020;127:522–33.

## Publisher's note